

Effect of Energy Band Gap in Graphene on Negative Refraction through the Veselago Lens and Electron Conductance

Dipendra Dahal¹ and Godfrey Gumbs^{1,2}

¹*Department of Physics and Astronomy, Hunter College of the City University of New York, 695 Park Avenue, New York, NY 10065, USA*

²*Donostia International Physics Center (DIPC), P de Manuel Lardizabal, 4, 20018 San Sebastian, Basque Country, Spain*

A remarkable property of intrinsic graphene is that upon doping, electrons and holes travel through the monolayer thick material with constant velocity which does not depend on energy up to about 0.3 eV (Dirac fermions), as though the electrons and holes are massless particles and antiparticles which move at the Fermi velocity v_F . Consequently, there is Klein tunneling at a $p-n$ junction, in which there is no backscattering at normal incidence of massless Dirac fermions. However, this process yielding perfect transmission at normal incidence is expected to be affected when the group velocity of the charge carriers is energy dependent and there is non-zero effective mass for the target particle. We investigate how away from normal incidence the combined effect of incident electron energy ϵ and band gap parameter Δ can determine whether a $p-n$ junction would allow focusing of an electron beam by behaving like a Veselago lens with negative refractive index. We demonstrate that there is a specific region in $\epsilon - \Delta$ space where the index of refraction is negative, i.e., where monolayer graphene behaves as a metamaterial. Outside this region, the refractive index may be positive or there may be no refraction at all. We compute the ballistic conductance across a $p-n$ junction as a function of Δ and ϵ and compare our results with those for a single electrostatic potential barrier and multiple barriers.

PACS numbers: 73.20.-r, 73.20.Mf, 78.20.Bh, 78.67.Bf

I. INTRODUCTION

Graphene is a virtually two-dimensional (2D) sheet of carbon atoms which is nearly transparent and a considerably strong material for its light weight, high thermal and electrical conductivity. It is an allotrope of carbon atoms with 2D properties. The atoms are packed densely in a regular sp^2 bonded atomic scale chicken wire hexagonal pattern. Creating high quality graphene is a complex process which prevented it from being easily available¹⁻³. However, recent work found that by analyzing graphene's interfacial adhesive energy, it is possible to separate graphene from the metallic background on which it is grown. With the experimental realization of graphene, the focus now is to obtain a thorough understanding of its electronic and photonic properties. In this regard, one of the most intriguing challenges of graphene is a comprehensive understanding of the transmission⁴⁻¹⁰ of charged particles across a potential barrier or a potential step.

In the case for transmission of an electron through a higher barrier than its incoming energy, the electron turns into a hole within the barrier region, with its momentum directed in the reversed direction, resulting in a negative refractive index¹¹⁻¹⁹ causing the electron beam to focus at a point, thereby producing a Veselago lens. There is always some probability for the electron to tunnel onto the other side of the barrier, which we have calculated in this paper. Our transmission probability is then employed in our calculation of the conductance²⁰⁻²². The behavior of the transmission coefficient as well as the conductance changes dramatically when an energy band gap is introduced in graphene which may be achieved either by placing the 2D monolayer on a substrate or exposing it to circularly polarized light^{23,24}.

The rest of our paper is organized as follows. In Sec. II, the σ_z model Hamiltonian is used to solve the Hamiltonian equation for the wavefunction in the various regions with a prescribed constant potential. Using the continuity condition for the wavefunction at an interface between regions, the transmission probability is calculated. This is carried out for a potential step, as well as for one and two electrostatic potential barriers. In Sec. III, we present numerical results for the transmission coefficient, and the conductance using the analytic results in Sec. II. We conclude our paper with some relevant remarks in Sec. IV.

II. THEORETICAL MODEL AND FORMULATION

A. Single Potential Step: n-p junction

First, we consider Dirac fermions with energy ϵ incident from the left-hand side of an electrostatic potential barrier at an angle θ_1 with respect to x -axis. This structure may be produced by applying a local top gate voltage to graphene. The model consists of regions “I” and “II”, with “II” denoting the step region and “I” the entry region into the potential step. The interface between the two regions is located at $x = 0$ as shown schematically in Fig. 1(a).

At low energy, the electronic properties of monolayer gapped graphene, although the microscopic Hamiltonian of carbon atoms is non-relativistic, are governed by a Dirac Hamiltonian given by

$$\mathcal{H} = \begin{pmatrix} \Delta + V(x) & v_F(\hat{p}_x - i\hat{p}_y) \\ v_F(\hat{p}_x + i\hat{p}_y) & -\Delta + V(x) \end{pmatrix}, \quad (1)$$

where $\hat{p}_\ell = -i\hbar\partial/\partial x_\ell$ with $x_\ell = x, y$ and v_F is the Fermi velocity. The energy eigenvalues are given by $\epsilon = V_\alpha \pm \sqrt{(\hbar v_F q_\alpha)^2 + \Delta^2}$ in region $\alpha = 1, 2$ with constant potential V_α and $q_\alpha = \sqrt{q_{\alpha,x}^2 + q_{\alpha,y}^2}$ is the magnitude of the wave vector in that region. Also, Δ is a parameter describing the energy band gap. Let θ_1 be the angle of incidence of the incoming electron with wave vector q_1 in region I and θ_2 is the angle of refraction in region II. The relationship between θ_1 and θ_2 is given by

$$\frac{\tan \theta_1}{\tan \theta_2} = s_2 \frac{|q_{2,x}|}{|q_{1,x}|} = s_2 \frac{\sqrt{\frac{(\epsilon - V_2)^2 - \Delta^2}{\hbar^2 v_F^2} - q_{2,y}^2}}{\sqrt{\frac{\epsilon^2 - \Delta^2}{\hbar^2 v_F^2} - q_{1,y}^2}}, \quad (2)$$

$$\frac{\sin \theta_1}{\sin \theta_2} = \frac{q_2}{q_1} = s_2 \sqrt{\frac{(\epsilon - V_2)^2 - \Delta^2}{\epsilon^2 - \Delta^2}}, \quad (3)$$

where $s_\alpha = \text{sgn}(\epsilon - V_\alpha)$, i.e. when $\epsilon < V_\alpha$, we are able to get negative refraction^{16–19}.

Making use of the Heisenberg equation of motion, the velocity operator can be evaluated as

$$\hat{v} = \dot{\mathbf{r}} = \frac{[\mathbf{r}, \mathcal{H}]}{i} = \hat{\sigma}. \quad (4)$$

The probability density for the state $|\psi\rangle$ is $|\psi|^2$ and the average probability current is denoted by $\mathbf{j}(\mathbf{r}, \mathbf{t})$. The conservation of probability is given by

$$\nabla \cdot \mathbf{j} + \frac{d|\psi|^2}{dt} = 0. \quad (5)$$

As the wave function is time-independent, we have $\nabla \cdot \mathbf{j} = 0$ and $\mathbf{j} = \Psi^\dagger \hat{\sigma} \Psi$. Also, the wavefunction in region α is represented by

$$\Psi_\alpha(x, y) = \left\{ a_\alpha e^{iq_{\alpha x} x} \begin{pmatrix} 1 \\ g_\alpha e^{i\theta_\alpha} \end{pmatrix} + r_\alpha e^{-iq_{\alpha x} x} \begin{pmatrix} 1 \\ g_\alpha e^{i(\pi - \theta_\alpha)} \end{pmatrix} \right\} e^{iq_{\alpha y} y}, \quad (6)$$

where

$$g_\alpha = s_\alpha \left\{ \frac{|\epsilon - V_\alpha| - \Delta}{\sqrt{(\epsilon - V_\alpha)^2 - \Delta^2}} \right\}. \quad (7)$$

Additionally, when $\epsilon < V_2$, inside the barrier region, the carrier electron is now in the valence band, transformed into a hole and for $\epsilon > V_2$, the particle is in the conduction band and maintains itself as an electron. For a step, we set $V_1=0$ and $V_2=V$. Using the continuity of the wave function at the interface and taking $a_1=1$, $r_2=0$ and $a_2=t$, we have

$$\begin{aligned} 1 + r_1 &= t, \\ g_1 e^{i\theta_1} + r_1 g_1 e^{i\pi - i\theta_1} &= t g_2 e^{i\theta_2}. \end{aligned} \quad (8)$$

Solving these simultaneous equations for t . we obtain

$$|t|^2 = \frac{4g_1^2 \cos^2 \theta_1}{g_1^2 + g_2^2 + 2g_1 g_2 \cos(\theta_1 + \theta_2)}. \quad (9)$$

In a state of stable equilibrium, the continuity equation yields current conservation which implies that

$$j_x(\text{incident}) + j_x(\text{reflected}) = j_x(\text{transmitted}) \quad (10)$$

from which we obtain

$$g_1 \cos \theta_1 - r_1^2 g_1 \cos \theta_1 = t^2 g_2 \cos \theta_2, \quad (11)$$

or

$$1 = r_1^2 + t^2 \frac{g_2 \cos \theta_2}{g_1 \cos \theta_1}. \quad (12)$$

From the conservation of probability, we have $R + T = 1$, where T is the transmission probability given by

$$T = |t|^2 \frac{g_2 \cos \theta_2}{g_1 \cos \theta_1} \quad (13)$$

and R is the reflection coefficient. Therefore, for gapped graphene, this gives us

$$T = \frac{4g_1 g_2 \cos \theta_1 \cos \theta_2}{g_1^2 + g_2^2 + 2g_1 g_2 \cos(\theta_1 + \theta_2)}. \quad (14)$$

When $\epsilon > V_2$ and the band gap is zero, this reduces to

$$T = \frac{2 \cos \theta_1 \cos \theta_2}{1 + \cos(\theta_1 + \theta_2)}. \quad (15)$$

However, when $\epsilon < V_2$ for gapless graphene, the angle θ_2 is replaced by $\theta_2 + \pi$.and we have instead

$$T = -\frac{2 \cos \theta_1 \cos \theta_2}{1 - \cos(\theta_1 + \theta_2)} \quad (16)$$

which agrees with the result in Ref. [19].

B. Single Potential Barrier: n-p-n junction

We now turn our attention to a model consisting of regions “I”, “II” and “III”, as shown in Fig. 1(b), with “II” denoting the barrier region and “I” and “III” the regions of entry and exit from the barrier, respectively. The boundaries of the barrier are located at $x = 0$ and $x = d$. Let θ_1 be the angle of incidence for the incoming electron with wave vector g_1 in region I. The corresponding wave functions for the electron in the three regions are

$$\begin{aligned}
\Psi_I(x, y) &= \left\{ A \begin{pmatrix} 1 \\ g_1 e^{i\theta_1} \end{pmatrix} e^{iq_1, xx} + B \begin{pmatrix} 1 \\ g_1 e^{i\pi - i\theta_1} \end{pmatrix} e^{-iq_1, xx} \right\} e^{iq_1, yy} , \\
\Psi_{II}(x, y) &= \left\{ C \begin{pmatrix} 1 \\ g_2 e^{i\theta_2} \end{pmatrix} e^{iq_2, xx} + D \begin{pmatrix} 1 \\ g_2 e^{i\pi - i\theta_2} \end{pmatrix} e^{-iq_2, xx} \right\} e^{iq_2, yy} , \\
\Psi_{III}(x, y) &= \left\{ E \begin{pmatrix} 1 \\ g_1 e^{i\theta_1} \end{pmatrix} e^{iq_1, xx} + F \begin{pmatrix} 1 \\ g_1 e^{i\pi - i\theta_1} \end{pmatrix} e^{-iq_1, xx} \right\} e^{iq_1, yy} .
\end{aligned} \tag{17}$$

In our notation, A, B, C, D, E and F are constants, $q_2^2 = \frac{(\epsilon - V_2)^2 - \Delta^2}{(\hbar^2 v_F^2)}$ is the square of the wave vector within the potential barrier $V_2 = V$ and, ϵ is the energy of the incident electron. Also, θ_1 is the angle which the incoming electron makes with the x -axis and θ_2 is the refracted angle inside the barrier. We have

$$\theta_2 = \tan^{-1} \left(\frac{q_2 \sin \theta_1}{\sqrt{(\epsilon - V_2)^2 - \Delta^2 - (q_2 \sin \theta_1)^2}} \right) \tag{18}$$

We now consider the case when there is a potential barrier ($n - p - n$ junction) for gapped graphene and the continuity of the wave function gives

$$\mathcal{M}_1 \begin{pmatrix} A \\ B \end{pmatrix} = \mathcal{N}_1 \begin{pmatrix} C \\ D \end{pmatrix} , \tag{19}$$

where,

$$\begin{aligned}
\mathcal{M}_1 &= \begin{pmatrix} 1 & 1 \\ g_1 e^{i\theta_1} & g_1 e^{i\pi - i\theta_1} \end{pmatrix} , \\
\mathcal{N}_1 &= \begin{pmatrix} 1 & 1 \\ g_2 e^{i\theta_2} & g_2 e^{i\pi - i\theta_2} \end{pmatrix} .
\end{aligned} \tag{20}$$

Transforming to a primed coordinate system by translating the origin to a new one at $x = d$, i.e. $x' = x - d$, we have, for region “II”

$$\begin{aligned}
\Psi_{II}(x, y) &= \left\{ C \begin{pmatrix} 1 \\ g_2 e^{i\theta_2} \end{pmatrix} e^{iq_2, xx'} e^{iq_2, xd} + D \begin{pmatrix} 1 \\ g_2 e^{i\pi - i\theta_2} \end{pmatrix} e^{-iq_2, xx'} e^{iq_2, xd} \right\} e^{iq_2, yy} , \\
&= \left\{ C' \begin{pmatrix} 1 \\ g_2 e^{i\theta_2} \end{pmatrix} e^{iq_2, xx'} + D' \begin{pmatrix} 1 \\ g_2 e^{i\pi - i\theta_2} \end{pmatrix} e^{-iq_2, xx'} \right\} e^{iq_2, yy} ,
\end{aligned} \tag{21}$$

where

$$\begin{pmatrix} C' \\ D' \end{pmatrix} = \begin{pmatrix} C e^{iq_2, xd} \\ D e^{-iq_2, xd} \end{pmatrix} = \begin{pmatrix} e^{iq_2, xd} & 0 \\ 0 & e^{-iq_2, xd} \end{pmatrix} \begin{pmatrix} C \\ D \end{pmatrix} . \tag{22}$$

Similarly, in region III,

$$\Psi_{III}(x, y) = \left\{ E' \begin{pmatrix} 1 \\ g_1 e^{i\theta_1} \end{pmatrix} e^{iq_1, xx'} + F' \begin{pmatrix} 1 \\ g_1 e^{i\pi - i\theta_1} \end{pmatrix} e^{-iq_1, xx'} \right\} e^{iq_1, yy} , \tag{23}$$

$$\begin{pmatrix} E' \\ F' \end{pmatrix} = \begin{pmatrix} E e^{iq_1, xd} \\ F e^{-iq_1, xd} \end{pmatrix} = \begin{pmatrix} e^{iq_1, xd} & 0 \\ 0 & e^{-iq_1, xd} \end{pmatrix} \begin{pmatrix} E \\ F \end{pmatrix} , \tag{24}$$

where

$$\begin{aligned}\mathcal{T}_{10} &= \begin{pmatrix} e^{iq_1,xd} & 0 \\ 0 & e^{-iq_1,xd} \end{pmatrix}, \\ \mathcal{T}_{1V} &= \begin{pmatrix} e^{iq_2,xd} & 0 \\ 0 & e^{-iq_2,xd} \end{pmatrix}.\end{aligned}\quad (25)$$

In the primed coordinate frame of reference, we have

$$\begin{pmatrix} 1 & 1 \\ g_2 e^{i\theta_2} & g_2 e^{i\pi-i\theta_2} \end{pmatrix} \begin{pmatrix} C' \\ D' \end{pmatrix} = \begin{pmatrix} 1 & 1 \\ g_1 e^{i\theta_1} & g_1 e^{i\pi-i\theta_1} \end{pmatrix} \begin{pmatrix} E' \\ F' \end{pmatrix}, \quad (26)$$

$$\begin{pmatrix} C' \\ D' \end{pmatrix} = \mathcal{N}_1^{-1} \cdot \mathcal{M}_1 \cdot \begin{pmatrix} E' \\ F' \end{pmatrix}, \quad (27)$$

where, in our notation,

$$\begin{aligned}\begin{pmatrix} C \\ D \end{pmatrix} &= \mathcal{T}_{1V}^{-1} \cdot \mathcal{N}_1^{-1} \cdot \mathcal{M}_1 \cdot \mathcal{T}_{10} \cdot \begin{pmatrix} E \\ F \end{pmatrix}, \\ \begin{pmatrix} A \\ B \end{pmatrix} &= \mathcal{M}_1^{-1} \cdot \mathcal{N}_1 \cdot \mathcal{T}_{1V}^{-1} \cdot \mathcal{N}_1^{-1} \cdot \mathcal{M}_1 \cdot \mathcal{T}_{10} \cdot \begin{pmatrix} E \\ F \end{pmatrix}.\end{aligned}\quad (28)$$

Setting $A = 1$, $E = t$ and $F = 0$, we obtain the transmission probability $T = |t|^2$ given by

$$T = \frac{4g_1^2 g_2^2 \cos^2 \theta_1 \cos^2 \theta_2}{4g_1^2 g_2^2 \cos^2 \theta_1 \cos^2 \theta_2 \cos^2(dq_2) + \sin^2(dq_2)(g_1^2 + g_2^2 - 2g_1 g_2 \sin \theta_1 \sin \theta_2)^2}, \quad (29)$$

This general result agrees with that in Ref. [4] for the special case of gapless graphene and we shall employ Eq. (29) in our numerical calculations presented below.

C. Two Potential Barriers

We now extend our formulation to calculations for two square potential barriers of equal height V , illustrated in Fig. 1(c). The first barrier is located between $x = 0$ and $x = d$ (region II) while the second barrier lies between $x = d + w$ and $x = 2d + w$ (region IV). The region between the barriers is denoted by region III, and to the far left and far right we have regions I and V, respectively. A straightforward calculation leads to the wave function for region III as

$$\Psi_{III}(x, y) = \left\{ E \begin{pmatrix} 1 \\ g_1 e^{i\theta_1} \end{pmatrix} e^{iq_1,xx} + F \begin{pmatrix} 1 \\ g_1 e^{i\pi-i\theta_1} \end{pmatrix} e^{-iq_1,xx} \right\} e^{iq_1,yy}. \quad (30)$$

Making use of,

$$\begin{pmatrix} E'' \\ F'' \end{pmatrix} = \begin{pmatrix} E e^{iq_1,x(d+w)} \\ F e^{-iq_1,x(d+w)} \end{pmatrix} = \begin{pmatrix} e^{iq_1,x(d+w)} & 0 \\ 0 & e^{-iq_1,x(d+w)} \end{pmatrix} \begin{pmatrix} E \\ F \end{pmatrix}, \quad (31)$$

we obtain,

$$\Psi_{III}(x, y) = \left\{ E'' \begin{pmatrix} 1 \\ g_1 e^{i\theta_1} \end{pmatrix} e^{iq_1,xx''} + F'' \begin{pmatrix} 1 \\ g_1 e^{i\pi-i\theta_1} \end{pmatrix} e^{-iq_1,xx''} \right\} e^{iq_1,yy}. \quad (32)$$

In a similar fashion, the wave function in the second barrier region (region IV) may be written as

$$\Psi_{IV}(x, y) = \left\{ G'' \begin{pmatrix} 1 \\ g_2 e^{i\theta_2} \end{pmatrix} e^{iq_{2,x}x''} + H'' \begin{pmatrix} 1 \\ g_2 e^{i\pi - i\theta_2} \end{pmatrix} e^{-iq_{2,x}x''} \right\} e^{-iq_{2,y}y}, \quad (33)$$

and

$$\begin{pmatrix} G'' \\ H'' \end{pmatrix} = \begin{pmatrix} e^{iq_{2,x}(d+w)} & 0 \\ 0 & e^{-iq_{2,x}(d+w)} \end{pmatrix} \begin{pmatrix} G \\ H \end{pmatrix}, \quad (34)$$

where G, H are constants and $x'' = x - (d + w)$. The wave function in the second barrier is also continuous at $x'' = 0$ i.e., at $x = d + w$ we must have:

$$\begin{pmatrix} E'' \\ F'' \end{pmatrix} = \mathcal{M}_1^{-1} \cdot \mathcal{N}_1 \cdot \begin{pmatrix} G'' \\ H'' \end{pmatrix} \quad (35)$$

which leads to

$$\begin{pmatrix} E \\ F \end{pmatrix} = \mathcal{T}_{20}^{-1} \cdot \mathcal{M}_1^{-1} \cdot \mathcal{N}_1 \cdot \mathcal{T}_{2V} \cdot \begin{pmatrix} G \\ H \end{pmatrix}, \quad (36)$$

with

$$\begin{aligned} \mathcal{T}_{20} &= \begin{pmatrix} e^{iq_{1,x}(d+w)} & 0 \\ 0 & e^{-iq_{1,x}(d+w)} \end{pmatrix}, \\ \mathcal{T}_{2V} &= \begin{pmatrix} e^{iq_{2,x}(d+w)} & 0 \\ 0 & e^{-iq_{2,x}(d+w)} \end{pmatrix}. \end{aligned} \quad (37)$$

Proceeding along lines like we employed above, we obtain the components of the wave function in region V as

$$\Psi_V(x, y) = \left\{ J \begin{pmatrix} 1 \\ g_1 e^{i\theta_1} \end{pmatrix} e^{iq_{1,x}x} + K \begin{pmatrix} 1 \\ g_1 e^{i\pi - i\theta_1} \end{pmatrix} e^{-iq_{1,x}x} \right\} e^{iq_{1,y}y}, \quad (38)$$

where J and K are constants. This may be rewritten as

$$\Psi_V(x, y) = \left\{ J^{iv} \begin{pmatrix} 1 \\ g_1 e^{i\theta_1} \end{pmatrix} e^{iq_{1,x}x^{iv}} + K^{iv} \begin{pmatrix} 1 \\ g_1 e^{i\pi - i\theta_1} \end{pmatrix} e^{-iq_{1,x}x^{iv}} \right\} e^{iq_{1,y}y}, \quad (39)$$

where $x^{iv} = x - (2d + w)$. Furthermore, in region IV, the wave function may be expressed in the following form:

$$\Psi_{IV}(x, y) = \left\{ G^{iv} \begin{pmatrix} 1 \\ e^{i\theta_2} \end{pmatrix} e^{iq_{2,x}x^{iv}} + H^{iv} \begin{pmatrix} 1 \\ e^{i\pi - i\theta_2} \end{pmatrix} e^{-iq_{2,x}x^{iv}} \right\} e^{iq_{2,y}y} \quad (40)$$

with

$$\begin{aligned} \begin{pmatrix} J^{iv} \\ K^{iv} \end{pmatrix} &= \begin{pmatrix} e^{iq_{1,x}(2d+w)} & 0 \\ 0 & e^{-iq_{1,x}(2d+w)} \end{pmatrix} \begin{pmatrix} J \\ K \end{pmatrix} \equiv \mathcal{T}_{30} \begin{pmatrix} J \\ K \end{pmatrix} \\ \begin{pmatrix} G^{iv} \\ H^{iv} \end{pmatrix} &= \begin{pmatrix} e^{iq_{2,x}(2d+w)} & 0 \\ 0 & e^{-iq_{2,x}(2d+w)} \end{pmatrix} \begin{pmatrix} G \\ H \end{pmatrix} \equiv \mathcal{T}_{3V} \begin{pmatrix} G \\ H \end{pmatrix}. \end{aligned} \quad (41)$$

Also, making use of the continuity condition at $x^{iv} = 0$, i.e., at $x = (2d + w)$, we obtain

$$\mathcal{N}_1 \begin{pmatrix} G^{iv} \\ H^{iv} \end{pmatrix} = \mathcal{M}_1 \begin{pmatrix} J^{iv} \\ K^{iv} \end{pmatrix} \quad (42)$$

and thus

$$\begin{pmatrix} G \\ H \end{pmatrix} = \mathcal{T}_{3V}^{-1} \cdot \mathcal{N}_1^{-1} \cdot \mathcal{M}_1 \cdot \mathcal{T}_{30} \cdot \begin{pmatrix} J \\ K \end{pmatrix}, \quad (43)$$

where

$$\begin{aligned} \mathcal{T}_{30} &= \begin{pmatrix} e^{iq_{1,x}(2d+w)} & 0 \\ 0 & e^{-iq_{1,x}(2d+w)} \end{pmatrix} \\ \mathcal{T}_{3V} &= \begin{pmatrix} e^{iq_{2,x}(2d+w)} & 0 \\ 0 & e^{-iq_{2,x}(2d+w)} \end{pmatrix}. \end{aligned} \quad (44)$$

So, we have a relationship between the pairs of coefficients (A, B) and (J, K) given by

$$\begin{pmatrix} A \\ B \end{pmatrix} = (\mathcal{M}_1^{-1} \mathcal{N}_1) \cdot (\mathcal{T}_{10}^{-1} \mathcal{M}_1^{-1} \mathcal{N}_1 \mathcal{T}_{1V})^{-1} \cdot (\mathcal{T}_{20}^{-1} \mathcal{M}_1^{-1} \mathcal{N}_1 \mathcal{T}_{2V}) \cdot (\mathcal{T}_{30}^{-1} \mathcal{M}_1^{-1} \mathcal{N}_1 \mathcal{T}_{3V})^{-1} \cdot \begin{pmatrix} J \\ K \end{pmatrix} \quad (45)$$

By induction, we have for $(N + 1)$ potential barriers

$$\begin{aligned} \begin{pmatrix} 1 \\ B \end{pmatrix} &= (\mathcal{T}_{00}^{-1} \mathcal{M}_1^{-1} \mathcal{N}_1 \mathcal{T}_{0V}) \cdot (\mathcal{T}_{10}^{-1} \mathcal{M}_1^{-1} \mathcal{N}_1 \mathcal{T}_{1V})^{-1} \cdot (\mathcal{T}_{20}^{-1} \mathcal{M}_1^{-1} \mathcal{N}_1 \mathcal{T}_{2V}) \\ &\times (\mathcal{T}_{30}^{-1} \mathcal{M}_1^{-1} \mathcal{N}_1 \mathcal{T}_{3V})^{-1} \cdots (\mathcal{T}_{(2N+1)0}^{-1} \mathcal{M}_1^{-1} \mathcal{N}_1 \mathcal{T}_{(2N+1)V}) \begin{pmatrix} t \\ 0 \end{pmatrix} \end{aligned} \quad (46)$$

Generalizing our formalism to $N + 1$ equally spaced potential barriers, our calculations show that

$$\mathcal{T}_{(2N+1)0} = \begin{pmatrix} e^{iq_{1,x}\{(N+1)d+Nw\}} & 0 \\ 0 & e^{-iq_{1,x}\{(N+1)d+Nw\}} \end{pmatrix} \quad (47)$$

$$\mathcal{T}_{(2N+1)V} = \begin{pmatrix} e^{iq_{2,x}\{(N+1)d+Nw\}} & 0 \\ 0 & e^{-iq_{2,x}\{(N+1)d+Nw\}} \end{pmatrix}. \quad (48)$$

Therefore, solving this equation for t , we obtain the transmission coefficient for multibarrier^{25,26} as $T = t \cdot t^*$. We now use these results to carry out our numerical calculations.

D. Conductance

The conductance coefficient²⁰ for a specific spin direction and valley across a potential step or potential barrier is given in terms of the transmission probability as follows:

$$G = \frac{e^2}{h} \int_0^{2\pi} d\theta T(\theta) \cos(\theta). \quad (49)$$

We shall employ this result below to investigate the behavior of the conducting properties of graphene under the influence of a split gate to produce an $n - p$ or $n - p - n$ junction. However, we must first analyze the transmission coefficient which we derived above in our formalism for gapped graphene.

III. NUMERICAL RESULTS AND DISCUSSION

In Figs. 2(a) and 2(b), we present polar plots for the transmission probability across a potential step for chosen incident energy in units of the barrier height and compare results for gapless and gapped graphene. Klein tunneling is evident at normal incidence when $\Delta = 0$ but there is some reflection in the case for gapped graphene. Off normal incidence, the transmission probability for gapless and gapped graphene again shows some differences which may also be significant, compared to head-on incidence for the electron beam. In Fig. 2(c), we also plot the angle of incidence as a function of the corresponding angle of refraction for chosen energy gap, thereby demonstrating the way in which negative refraction is affected by an energy gap in monolayer graphene. We also exhibit in Fig. 2(d) a density plot for the transmission probability across a potential step as a function of incident angle and energy for gapped monolayer graphene. Our results clearly show that there is a forbidden energy region for incoming electrons at any angle and that these results differ substantially from those corresponding to tunneling across a potential barrier¹⁹.

Figures 3(a), 3(b), 3(c) and 3(d) illustrate the changes in the transmission probability for different incident energy of an electron impinging on a single potential barrier for gapped and gapless graphene with chosen barrier width. Unlike gapless graphene, for normal incidence in gapped graphene, the transmission probability oscillates as the energy is varied in Fig. 3(a) and its value drops drastically when the incident energy is close to the barrier height. The polar plots in the Fig. 3(b) and for the chosen barrier width show that Klein tunneling is suppressed at normal incidence, thereby illustrating some possible reflection even for zero angle of incidence. We also present in Figs. 3(c), (d) the transmission results in the form of density plot as a function of incident energy and the angle of incidence. The results show the brighter region corresponding to higher transmission probability and there is the region in the middle of the figure where transmission is not allowed for some values of energy for any angle of incidence when there is a band gap.

We now turn our attention to the transmission of an electron through two electrostatic potential barriers separated by some distance w . Our results are presented in Figs. 4(a), 4(b), 4(c) and 4(d). The inter-barrier separation leads to polar plots which, as expected, bear similarities with that obtained in Fig. 3, with forbidden regions of transmission for some range of energy and incident angle. However, unlike the case for a single barrier, we observe some bright regions in the middle section of the density plot. These spikes are due to the commensurability oscillations of the waves in between the barriers. The spike locations depend on the parameters chosen for the barrier width as well as the energy band gap.

We have made use of our results for the transmission probability to calculate the ballistic conductance for all the above mentioned geometries. For a potential step, Fig. 5(a) shows the conductance as a function of the energy gap parameter Δ for chosen values of incoming electron energy. Here, the conductance is almost constant for small Δ/V and it falls precipitously when the band gap parameter is close to the electron incident energy. Figure 5(b) shows the variation of the conductance coefficient with incident electron energy for various values of band gap. For the range of energy shown, the conductance decreases monotonically with energy when $\Delta = 0$. However, when there is an energy band gap, there is conductance only when $\epsilon > \Delta$ as required for graphene electrons in the conduction band. This requirement leads to the expected behavior of conductance in Figs. 5 (a) and (b).

We vividly demonstrate in Fig. 6 that there is a relationship between the electron energy ϵ and band gap parameter Δ showing the region in $\epsilon - \Delta$ space when there is focusing of an electron beam across a potential step in monolayer graphene. Thus, we have identified a limited region where the refractive index is negative. Outside this region, the refractive index may either be positive (transmission without focusing) or there is no transmission at all, i.e., the equation governing refraction may not be satisfied, to yield real solutions for Eq. (3). In particular, these results show that for gapless graphene, the range of energy for negative refraction is larger than for gapped graphene. This dramatic result from our theory means that one may specifically choose negative refractive index by allocating the band gap.

We present novel results for the $n - p - n$ conductance as functions of the energy gap parameter Δ , the incident energy ϵ and the barrier width d in Figs. 7(a), 7(b) and 7(c), respectively. Unlike the results in Fig. 5 for a potential step, in an $n - p - n$ junction, the conductance in Fig. 7(b) has characteristic commensurability oscillations due to the ratio between the de Broglie wavelength and the barrier width. The reflections at the barrier interface change a smooth curve in Fig. 5(b) into a decreasing, oscillating curve in Fig. 7(b) for the conductance as a function of the energy parameter ϵ . It is evident that commensurability oscillations for an $n - p - n$ junction are superimposed on the $n - p$ junction conductance results, including a lower bound on the existence of this transport coefficient. We also note that Fig. 7(b) shows that for finite energy gap, there is a range of energy for which the conductance is zero and that this range of energy for an insulating phase increases with Δ . Figure 7(c) clearly demonstrates the commensurability oscillations as the barrier width is varied.

Based on the formula for the conductance, we carried out calculations across two potential barriers as shown in Figs. 8(a) and 8(b). As the energy is increased, the conductance shows a periodic oscillations and we observe a dip in the conductance when the electron energy is close to the barrier height. This is because of the drop in the transmission probability in that regime. As for an $n-p-n$ junction, the conductance does not exist for energy less than the band gap parameter Δ and for the difference between the electron energy and the barrier height less than Δ . Figure 8(b) shows the conductance versus barrier width. As in the case of an $n-p-n$ junction, the conductance falls off from a high to a reduced value for the lower barrier width. As the width is increased, the conductance oscillates as shown in Fig. 8(b). When the band gap is finite, the average conductance is decreased as the band gap is increased.

IV. CONCLUDING REMARKS

The interaction between Dirac particles in graphene and circularly polarized light leads to the formation of quantum electron dressed states with an energy band gap of order 50 meV. This gap may be produced by the application of laser light of suitable power. So, because of the creation of a band gap between the valence and conduction bands in graphene, we do not see the Klein tunneling for normal incidence of an electron beam. Instead, we observe complete transmission at some other angle of incidence. When there are two or more potential barriers present, we observe that the number of peaks in the transmission spectrum increases. This is due to interference between oppositely traveling waves within a barrier and between separated barriers. The interference effect is reduced when the barriers are brought closer together.

An important result coming out of our calculations is that there is a well defined region in $\epsilon-\Delta$ space where negative refraction, i.e., focusing of an electron beam, may occur for monolayer graphene when a negative-positive split gate is applied. Outside this region, the beam may not be refracted at all or, if there is refraction, the refractive index may be positive. This means that by varying the energy band gap appropriately, we could have a selected refractive index for monolayer graphene. Our conductance calculations show that there is a lower bound for the incident energy for gapped graphene with a $p-n$ junction, thereby indicating a metal-insulator transition. The regions of finite refraction in Fig. 6 determine the range for the incident energy and gap for monolayer graphene where the conductance is finite in Fig. 5(a). When a potential barrier is introduced, our calculations show that there are commensurability oscillations superimposed on the conductance curves for a step due to interference between incident and reflected waves from the potential walls. Therefore, our present work plays an important role in demonstrating that monolayer graphene may serve as a metamaterial only in a well-defined range of electron energy and band gap, i.e., focusing may be achieved in a limited region of $\epsilon-\Delta$ space when a positive-negative bias is applied. The conductance for monolayer graphene with an electrostatic barrier or multiple barriers reveals interference effects due to the ratio of the de Broglie wavelength to the barrier width.

-
- ¹ C. Y. Su, A. Y. Lu, Y. Xu, F. R. Chen, A. N. Khlobystov, and L. J. Li, ACS Nano, **5**, 2332 (2011).
 - ² K. S. Kim, Y. Zhao, H. Jang, S. Y. Lee, J. M. Kim, K. S. Kim, J. H. Ahn, P. Kim, J. Y. Choi and B. H. Hong, Nature **457**, 706-710 (2009).
 - ³ W. Bao, G. Liu, Z. Zhao, H. Zhang, D. Yan, A. Deshpande, B. LeRoy, and C. N. Lau, Nano Research **3**, 98-102 (2010).
 - ⁴ A. H. C. Neto, F. Guinea, N. M. R. Peres, K. S. Novoselov and A.K.Geim, Rev. Mod. Phys.**81**, 109(2009).
 - ⁵ M. I. Katsnelson, K. S. Novoselov, and A. K. Geim, Nature Phys. **2**, 620-625 (2006).
 - ⁶ O. V. Kibis, Phys. Rev. B **81**, 165433 (2010).
 - ⁷ A. Iurov, Godfrey Gumbs, O. Roslyak and D. Huang, J.Phys. Condens. Matter **24**, 015303 (2011).
 - ⁸ L. G. Wang and S. Y. Zhu, Phys. Rev. B, **81**, 205444 (2010).
 - ⁹ J. M. Pereira, F. M. Peeters, A. Chaves and G. A. Farias, Semicond. Sci. Tech, **25**,033002 (2010).
 - ¹⁰ J. M. Pereira, P. Vasilopoulos, F. M. Peeters, Appl. Phys. Lett. **90**, 132122 (2007).
 - ¹¹ C. W. J. Beenakker, Rev. Mod. Phys. **80**, 1337 (2008).
 - ¹² K. V. Sreekanth, A. De Luca, and G. Strangi, AIP, Apl. Phys Lett., **103**, 023107 (2013).
 - ¹³ J. J. Cserti, A. Palyi, and C. Peterfalvi, Phys, Rev. Lett. **99**, 246801 (2007).
 - ¹⁴ S. A. Ramakrishna, Rep. Prog. Phys. **68**, 449 (2005).
 - ¹⁵ J. B. Pendry, Science, **322**, 71-73 (2008).
 - ¹⁶ V. V. Cheianov, V. Falko and B. L. Altshuler, Science, **315**, 1252-1255(2007).
 - ¹⁷ V. G. Veselago, Soviet Physics Uspekhi, **10**, 509(1968).
 - ¹⁸ J. B. Pendry, Phys Rev. Lett. **85**, 3966 (2000).
 - ¹⁹ P. E. Allain, J. N. Fuchs, Eur. Phys. Jour. B, **83**, 301 (2011).
 - ²⁰ V. Vargiamidis and P. Vasilopoulos, Appl, phys. Lett. **105**, 223105 (2014).

- ²¹ M. Barbier, P. Vasilopoulos, F. M. Peeters, and J.M.Pereira, Phys. Rev. B **79**, 155402 (2009).
- ²² M. Barbier, P. Vasilopoulos and F. M. Peeters, Phys. Rev. B **81**, 075438 (2010).
- ²³ S. Y. Zhou, G. H. Gweon, A. V. Fedorov, P. N. First, W. A. de Heer, D.-H. Lee¹, F. Guinea, A. H. Castro Neto, and A. Lanzara, Nature materials, **6**, 770-5 (2007).
- ²⁴ M. Y. Han, B. Ozyilmaz, Y. Zhang, and P. Kim, Phys. Rev. Lett., **98**, 206805 (2007).
- ²⁵ S. Esposito, Phys. Rev. E **67**, 016609 (2003).
- ²⁶ W. T. Lu, S. J. Wang, W. li, Y. L. Wang, and H Jiang, Physica B **407**, 918-921 (2012).

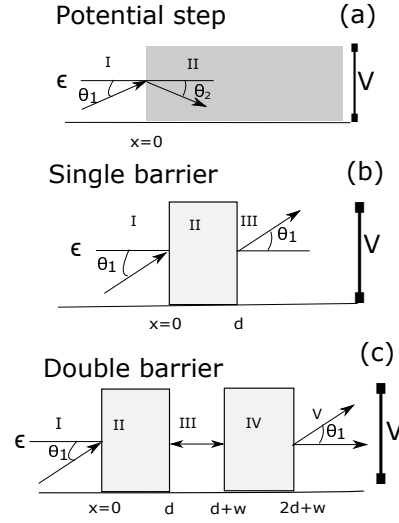


FIG. 1: (Color online) Schematic representation of (a) a step potential, $\epsilon < V$, (b) a single potential barrier, and (c) a pair of potential barriers.

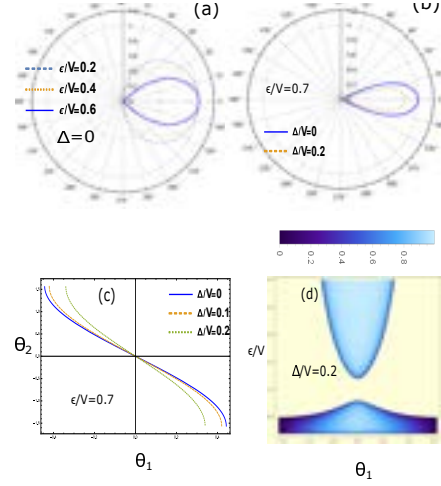


FIG. 2: (Color online) Polar plots of the transmission coefficient at different incident energies for (a) gapless and (b) gapped graphene for chosen incident energy. In (c), we show the relationship between the angle of incidence and the angle of refraction for chosen energy gap and incident energy. Density plot of the transmission coefficient across a step is shown in (d) as a function of the angle of incidence and energy.

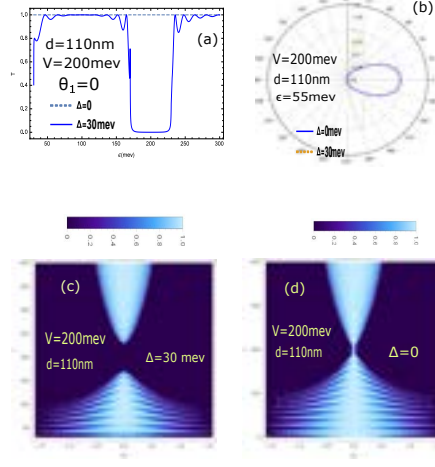


FIG. 3: (Color online) (a) Plots for the transmission probability of an electron through a single potential barrier versus the incident energy. In (b), polar plots are presented for transmission for different angles of incidence. Panels (c) and (d) respectively show transmission density plots for gapped and gapless graphene.

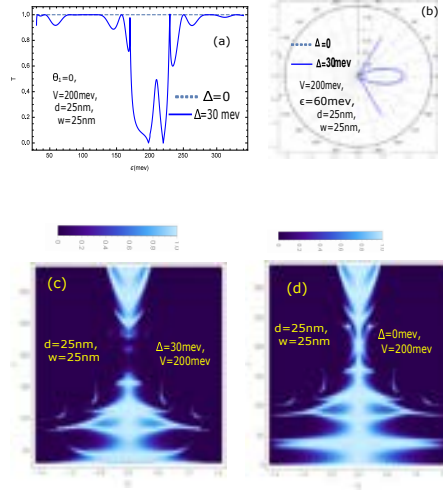


FIG. 4: (Color online) Transmission probability through two potential barriers. All parameter for the barrier height, and energy band gap are the same as in Fig. 3. But, here the barrier width $d=50\text{nm}$ and the inter-barrier separation $w=50\text{nm}$.

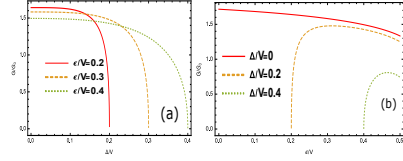


FIG. 5: (Color online) Conductance plots, in units of $G_0 = e^2/h$, for gapped and gapless graphene when there is a step potential. Panel (a) shows the conductance versus the band gap parameter for chosen energy. Panel (b) presents how the conductance varies with incident energy for chosen band gap.

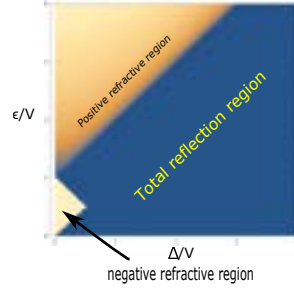


FIG. 6: (Color online) Density plot of limited negative refractive index as a function of incident energy and energy band gap.

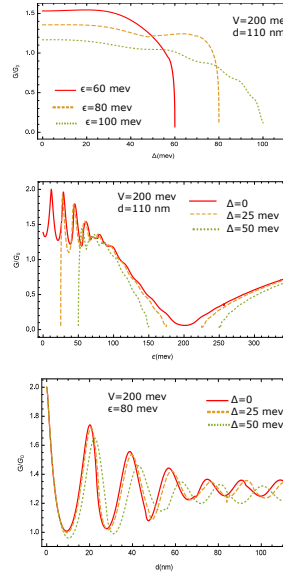


FIG. 7: (Color online) Conductance plots for ballistic transport for gapped and gapless graphene when there is only one potential barrier. The conductance coefficient is plotted as a function of (a) the energy band parameter Δ , (b) incident energy ϵ , and (c) potential barrier width d .

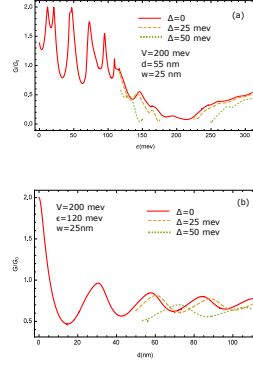


FIG. 8: (Color online) Conductance plots, in units of $G_0 = e^2/h$, for gapped and gapless graphene when there is a pair of potential barriers. Panel (a) shows the conductance as a function of the incident electron energy for chosen band gap with barrier width $d=55nm$ and inter-barrier separation $w=25$ nm. Panel (b) shows conductance versus barrier width for chosen parameter values as indicated in the figure.